



UNIVERSITÀ
DEGLI STUDI
FIRENZE

FLORE

Repository istituzionale dell'Università degli Studi di Firenze

Design guidelines for H-Darrieus wind turbines: Optimization of the annual energy yield

Questa è la Versione finale referata (Post print/Accepted manuscript) della seguente pubblicazione:

Original Citation:

Design guidelines for H-Darrieus wind turbines: Optimization of the annual energy yield / Alessandro Bianchini;Giovanni Ferrara;Lorenzo Ferrari. - In: ENERGY CONVERSION AND MANAGEMENT. - ISSN 0196-8904. - STAMPA. - 89:(2015), pp. 690-707. [10.1016/j.enconman.2014.10.038]

Availability:

This version is available at: 2158/914938 since: 2021-03-30T14:31:58Z

Published version:

DOI: 10.1016/j.enconman.2014.10.038

Terms of use:

Open Access

La pubblicazione è resa disponibile sotto le norme e i termini della licenza di deposito, secondo quanto stabilito dalla Policy per l'accesso aperto dell'Università degli Studi di Firenze (<https://www.sba.unifi.it/upload/policy-oa-2016-1.pdf>)

Publisher copyright claim:

(Article begins on next page)

Design guidelines for H-Darrieus wind turbines: optimization of the annual energy yield

Alessandro BIANCHINI^{1a}, Giovanni FERRARA^{1b}, Lorenzo FERRARI^{2c*}

¹⁾ Department of Industrial Engineering, University of Florence

Via di Santa Marta 3, 50139, Florence, Italy

Phone +39 055 4796 570 - Fax +39 055 4796 342

²⁾ CNR-ICCOM, National Research Council of Italy

Via Madonna del Piano 10, 50019, Sesto Fiorentino, Italy

* Phone +39 055 5225 218 - Fax +39 055 5225 203

Abstract

H-Darrieus wind turbines are gaining popularity in the wind energy market, particularly as they are thought to represent a suitable solution even in unconventional installation areas. To promote the diffusion of this technology, industrial manufacturers are continuously proposing new and appealing exterior solutions, coupled with tempting rated-power offers. The actual operating conditions of a rotor over a year can be, however, very different from the nominal one and strictly dependent on the features of the installation site.

Based on these considerations, a turbine optimization oriented to maximize the annual energy yield, instead of the maximum power, is thought to represent a more interesting solution. With this goal in mind, 21600 test cases of H-Darrieus rotors were compared on the basis of their energy-yield capabilities for different annual wind distributions in terms of average speed.

a) bianchini@vega.de.unifi.it

b) ferrara@vega.de.unifi.it

c) lorenzo.ferrari@iccom.cnr.it (corresponding author)

The wind distributions were combined with the predicted performance maps of the rotors obtained with a specifically developed numerical code based on a Blade Element Momentum (BEM) approach. The influence on turbine performance of the cut-in speed was accounted for, as well as the limitations due to structural loads (i.e. maximum rotational speed and maximum wind velocity). The analysis, carried out in terms of dimensionless parameters, highlighted the aerodynamic configurations able to ensure the largest annual energy yield for each wind distribution and set of aerodynamic constraints.

Keywords

Darrieus, VAWT, wind turbine, design, energy yield, aerodynamics

1. Introduction

In 2011, the wind energy market grew by 6% compared to 2010, despite the economic and political turmoil in Europe and North America, with a newly installed power of 40.5 GW [1].

The great bulk of installed wind energy plant is today in the form of large wind farms [2] which mainly comprehend large Horizontal Axis Wind Turbines (HAWTs) feeding into power supply grids: turbines are becoming more and more efficient and a scale-up tendency is clearly distinguishable. Moreover, technological improvements in design and efficient maintenance have considerably reduced their operating cost and consequently disclosed new diffusion frontiers like the offshore applications [3-4]. Whereas these installations are a valuable addition to the grid capacity, they actually do not benefit people who are not served by grids. As a consequence, much interest is being paid to understand where wind turbines can effectively represent an alternative for delocalized power production [5-6]. Paradoxically, however, there has been very little research and commercial development in the second part of the century on small stand-alone systems, although great improvements in the blade aerodynamic design have been made. In recent times, a reversal of this trend has been fortunately experienced.

Increasing interest is especially being paid by architects, project developers and local governments to understand where small wind turbines can effectively be exploited to provide delocalized power in the built environment (e.g. see Refs. [7-12]). The real feasibility of this scenario has, however, yet to be proved, both in terms of real energy harvesting and of compatibility of the machines with a populated area [9-10,13].

In particular, Vertical-Axis Wind Turbines (VAWTs), both drag [14-16] and lift-driven [17-20], are gaining popularity in the wind energy scenario, especially in medium and small-size installations, where they can work effectively even in presence of low-speed and unstructured flows with low noise emissions and high reliability. Among others, H-Darrieus rotors are increasingly appreciated in unconventional contexts as they are even assumed to increase their performance in case of an oncoming flow misaligned with respect to the axis of the rotor [17-19]. In order to promote the diffusion of this technology, on one hand, industrial manufacturers are developing new and more appealing design solutions (e.g. [21-25]); on the other hand, efforts are being devoted to reducing the initial cost of the machines (primarily by means of new materials) and to increasing the efficiency, in order to make them competitive with respect to more conventional Horizontal Axis Wind Turbines (HAWTs) [20].

Focusing on the commercial aspects, it is also worth pointing out that almost all the industrial rotors are generally designed and optimized for a specific wind speed (i.e. the speed which ensures the highest energy production), but the rated power values, which are often perceived by the final customer as the most valuable indicator of the quality of the product, are declared for their nominal wind velocity, i.e. the highest functioning speed, which provides the maximum power production. Although the importance of accounting for energy instead of power does not come as a surprise for the applied-energy technicians, the implications of this theoretical dichotomy are quite often not completely understood by the final customer of small and medium wind turbines.

In detail, the actual operating conditions of a rotor over a year can indeed be very far from the nominal one [9-10,26]. In particular, the available wind energy can be concentrated at the lower wind velocities of the yearly distribution in the installation site, which can be often correctly approximated by a Weibull function [27-30]; in addition, the specific features of the final environment (e.g. local accelerations, effects of obstacles, etc.) are very important in determining the real characteristics of the flow which effectively invests the rotor (e.g. [9-10]). As a result, a turbine optimized only for a singular wind speed could provide poor performance during the largest part of its operating time, with a remarkable reduction of the energy produced and, consequently, of the suitability of the investment [10].

Stated the above, a design approach based on the maximization of the annual energy-yield (i.e. the sum of the energy contributions at all the wind speeds experienced over the year) was thought to represent a more valuable solution.

2. Energy-yield-based design strategy

The main goal of this study was to define some effective design guidelines for Darrieus wind turbines which would be able to ensure the maximum energy harvesting in a yearly horizon as a function of the attended wind distribution in the installation site.

With this goal in mind, 21600 test cases, i.e. permutations of a specific geometrical configuration (300 cases), an airfoil (4 selections), a wind distribution (6 cases) and a load system (3 cases), were tested and analyzed by means of a specifically developed numerical code based on an advanced BEM method, in order to highlight the configurations which ensure the largest annual energy yield for each wind condition.

2.1 Wind distributions

As a first step of the analysis, six annual wind profiles were hypothesized. As discussed, the most logical representation of the annual wind distribution must be based on the assumption of a Weibull distribution [27-30]. In particular, in the present study a constant shape factor equal

to 2.0 (Rayleigh distribution) was considered, whereas the scale factor was modified in each case in order to ensure an average wind speed (\bar{U}) increasing by one from 3 to 8 m/s.

The choice of the Rayleigh distribution was based on literature data [9-10], which found that this particular Weibull curve nicely approximates the wind distributions of some medium-low velocity sites in Europe. The presented method, however, is of general validity and can be applied to any Weibull distribution attended in the installation site.

In further detail, the wind profiles investigated in this study are shown in Figure 1, where the cut-in and the cut-out limits are also displayed. In particular, it is worth pointing out that a maximum cut-out velocity of 18 m/s was imposed for safety reasons to all the tested rotors [26], based on the industrial experience for these rotors. On the other hand, the cut-in speed was specifically calculated for each rotor on the basis of its behavior at low wind speeds: as shown by Figure 1, a variable cut-in speed between 2 and 3 m/s was measured in the tested rotors. In particular, it is worth pointing out that in the present study the attention was focused only on the Darrieus machines, evaluating their actual self-starting characteristics. Although recent studies (e.g. [31-32]) showed indeed that the self-starting can be enhanced by coupling these rotors with drag-driven devices, the matching of the two turbines was not considered in the scope of the present work and destined to further studies.

2.2 Main design parameters for Darrieus-type turbines

The proper set of rotor configurations to be analyzed was then defined. Due to the large number of variables involved in the aerodynamic design of Darrieus rotors [20,26], some preliminary assumptions were needed to focus the analysis on a significant family of turbines.

In particular, the following main choices were made:

- The H-Darrieus configuration with straight blades was selected (see Figure 2). This turbine shape is presently the most exploited and studied solution in Darrieus turbines design, due to higher efficiency and lower manufacturing costs with respect to original troposkien-bladed rotors [20,24,33].

▪ A blades number $N=3$ was assumed. This turbine's architecture guarantees a good efficiency and a sufficiently flat torque profile during revolution, without compromising solidity [20,23-24].

▪ At least two supporting struts for each blade were applied (the number was increased by one strut for each blade whenever too high structural stresses were calculated) [21,26].

On these bases, the resulting performance maps must be related only to this typology of rotors and future works will be devoted at extending the validity range of the analyses.

Then, some significant design parameters to be investigated were chosen [26]. In order to define a set of parameters able to provide a prompt description of the geometrical proportions of the rotor, the attention was focused on:

▪ The *height/diameter ratio* ($\Phi=H/D$);

▪ The *chord/diameter ratio* ($\xi=c/D$);

▪ The *swept area* of the rotor (A);

▪ The airfoil type;

▪ The struts dimensions.

In order to understand the aerodynamic implications of these parameters, one has to focus on the physical functioning of Darrieus rotors. In particular, if it is generally well understood that a rotational axis perpendicular to the flow actually results in a flow incidence continuously variable during the revolution, the influence of the chord-based Reynolds number on the airfoils (Eq.1) is generally underestimated, especially in small and medium rotors.

$$Re_c = \frac{wC}{\nu} \quad (1)$$

In further details, when small-sized rotors are designed, the Reynolds number can be very low (especially in case of low wind speeds), even lower than 10^5 , being therefore very critical for a correct airfoil functioning.

A suitable Re_c on the blade can be achieved through different ways. Assuming that the wind speed cannot be altered (i.e. a specific wind speed is analyzed), the most intuitive solution

would consist in a direct increase of the chord c (Eq. 1). This solution is definitely able to accomplish the goal, but strict limitations to its use must be introduced. In particular, notably longer chords produce both a reduction of the Aspect Ratio of the blade (i.e. the ratio between the blade length and the chord - Eq. 2) and an increase of the solidity of the rotor (Eq. 3) [21,24,26].

$$AR_b = \frac{H}{c} \quad (2)$$

$$\sigma = \frac{Nc}{D} \quad (3)$$

The first effect actually results in a detriment of the blade efficiency [18,21], as the increase of the rotor's height to compensate cannot be always provided as the swept area of the rotor is generally a priori selected (Eq.4 for an H-Darrieus).

$$A = H \cdot D \quad (4)$$

On the other hand, an increase of the solidity also produces a reduction of the peak efficiency of the rotor [20,21,24], which once more cannot be simply compensated by reducing the diameter because this countermeasure would directly reduce the peripheral speed, thus leading to an undesired reduction of the relative speed W (given by the vector sum of the peripheral speed and the wind speed reduced by the induction factor a - see Eq.5):

$$W = \omega R + U(1 - a) \quad (5)$$

The second way to control the Reynolds number on the blade is in fact the modification of the relative speed. Having assumed that the wind speed U is fixed, the only way to modify w is related to a variation of the peripheral speed ωR .

Analogous to the previous analysis a double choice is given. An increase of the turbine radius would directly improve the Reynolds number: being A fixed, the turbine's height would be reduced (Eq. 4) and then the Aspect Ratio of the blades (Eq.2), leading to less efficient blades. On the other hand, increasing the revolution speed would improve the relative speed, having,

however, a notable impact on the incidence angles range and the structural behavior of the rotor.

Based on the above, the influence of the selected parameters can be readily highlighted.

- **Φ ratio** - The Φ ratio has a double effect in defining the features of the rotor. From an aesthetic point-of-view, it can be considered as a “shape factor” of the turbine, i.e. an indicator of the visual proportions of the virtual cylinder swept during the revolution. On the other hand, for a fixed swept area, low Φ values are typical of a machine in which the optimal flow conditions on the airfoil are obtained thanks to large diameters in order to increase the peripheral speed. In this configuration, the velocity triangles on the airfoils are improved but the blades are generally short, with more relevant losses due to end-effects. Conversely, high Φ values can be related to machines in which the efficiency of the blade (high blade Aspect Ratios - Eq. 2) is preferred.

- **ξ ratio** - The c/D ratio is a direct indicator of the solidity (σ) of the rotor (Eq. 3). High values of ξ generally indicate that the chord length is increased to improve the Reynolds number, whereas low ξ values can be related to rotors in which the relative wind speed is increased by means of an increase of the relative wind speed on the airfoil (Eq. 5).

- **Swept Area (A)** - As one can argue from the previous discussion, the swept area of the turbine (Eq. 4 - valid for an H-Darrieus rotor) is unfortunately a dimensional parameter which cannot be bypassed in the analysis of small rotors. In particular, larger swept areas ensure less demanding limits of the turbine’s radius, ensuring higher peripheral speed and, therefore, fewer problems in ensuring a good Reynolds number on the blades. Moreover, being the optimal solidity ranges generally constant [20-21], the minimum requested chords are generally smaller, resulting in higher Aspect Ratios and more efficient blades.

- **Design variables** - The airfoil type is very important in defining the performance of a Darrieus turbine; as a result, the dimensionless analysis on the best design trends must be individually carried out for each specific airfoil family [20,34-35]. Finally, the struts’

shape and dimensions must be carefully taken into account as they can substantially modify the power output of an H-Darrieus rotor (see Refs. [21,24,33,36]) due to the parasitic torque that is produced during the revolution. To this purpose, the impact of the struts was also included in this study by assuming a variation of their dimensions, and even number, as a function of the structural stresses on the blades.

3. Test plan and design parameters

The test plan of the investigated configurations is summarized in Table 1.

The limits of the ξ and Φ parameters were defined on the basis of a survey of the technical literature (e.g. [5,20,24]). In particular, the ξ range was limited to 0.200 as higher values would lead to solidities higher than 0.6. Design choices over this limit are in fact considered to be unsuitable for H-Darrieus rotors [20,24], due to the fact that the turbine is deemed to become similar to a solid obstacle for the wind and the interactions between upwind and downwind blades becomes so strong to compromise the aerodynamics of the airfoils. In addition, the theory applied in the simulations could become less predictive in similar test-cases [20].

The choice of the aerodynamic airfoils was also based on a literature survey [5,20-21]. In particular, four different airfoils were investigated in this work, in order to highlight the impact of their aerodynamic characteristics on the effective energy harvesting of the turbine. The airfoils were selected among the 4-digit NACA family, which is quite a conventional solution in Darrieus VAWTs [5,20,34-35].

In detail, three uncambered airfoils with different thickness/chord ratios (NACA0012, NACA0015, NACA0018) were compared to an asymmetrical and lightly-cambered airfoil (NACA4415). The first group of airfoils is a widely exploited solution in Darrieus turbines, as it ensures a suitable resistance to the stall coupled with good lift outputs at medium-range Reynolds numbers. Moreover, a symmetric airfoil is able to provide the same lift contribution either with positive or negative incidence [20,24]. On the other hand, a cambered profile, like the selected NACA4415, has been suggested in technical literature (e.g. see [5,21]) as an

interesting design choice in order to ensure high peak values of the torque in low-velocity cases, although some doubts on their effective application are due to the different behaviour of a non-symmetric airfoil in case of a positive or negative incidence [21].

Focusing on the boundary conditions in terms of loads applied to the rotor, three different configurations were analyzed:

- **CASE 1 – Aerodynamics only:** in this configuration, the contribution of the resistant torque of the struts was not considered. By doing so, this configuration actually refers to a hypothetical solution of a fully aerodynamic relationship between the geometrical features of the rotor and the power performance. Although not practically applicable, the analysis of these results allows one to define the aerodynamic trends and to directly compare the functioning behavior of machines having different areas. Moreover, by defining the purely aerodynamic requests, one can also directly identify the effects induced by the secondary and parasitic effects due to auxiliary organs (e.g. the struts) and external loads.
- **CASE 2 – Centrifugal load:** the contribution of the resistant torque of the struts was again not considered but a limitation on the centrifugal stress acting on the blades was added as a function of the rotational speed of each model.
- **CASE 3 – Struts' parasitic torque:** in this latter configuration, both a limitation on the centrifugal stress on the blades and variable struts dimensions, as a function of the rotational speed of each model, were included. Moreover, the resistant torque of the struts was taken into account.

In order to give a correct estimation of the structural loads, in this study a manufacturing technology based on extruded aluminium blades with a hollowed section was considered, utilizing real data on both the maximum centrifugal stress and on the maximum mechanical stress on the struts available from previous design experiences of the authors [33].

In further detail, in Case 2 the cut-out speed of the turbine was calculated in each case-study based on the hypothesis that the maximum centrifugal stress at the middle of the blade (where

the maximum displacement is located) would not exceed a fixed stress limit of the blade itself (Eq. 6).

$$\varsigma_b = \frac{F_b}{A_{res_b}} = \frac{m_b \omega^2 R}{A_{res_b}} \leq \varsigma_{lim_b} \quad (6)$$

where A_{res_b} is a conventional resistance area which takes into account the structure of the stiffeners inside the airfoil and F_b is the centrifugal stress of the blade of mass m_b . In particular, all the airfoils were reproduced with a hollowed section having a constant skin thickness (3 mm) and three, equally spaced, rectangular stiffeners perpendicular to the chord of variable thickness. The trailing edge was considered as solid with a fillet radius increasing proportionally to the chord of the blade (Figure 3). Based on the characteristics of an aluminium alloy tested by the authors in a previous industrial experience [33,37], a stress limit of 90 N/mm² was here considered.

In addition, in Case 3 even the dimensions of the struts (at least two for each blade) are variable from one configuration to another in order to satisfy the stress limit of the blades due to the centrifugal force (Eq. 7 with the same notation of Eq. 6).

$$\varsigma_{ST} = \frac{F_{ST}}{A_{res_ST}} = \frac{1}{N_{ST}} \frac{m_b \omega^2 R}{A_{res_ST}} \leq \varsigma_{lim_ST} \quad (7)$$

It is worth pointing out that the load case considered in Eq. 7 takes into account only the tensile stresses generated by the centripetal acceleration of the rotor. In authors' experience (see [33,37]), this load condition is quite realistic for small-size rotors (i.e. with a swept area up to 4.0 m²), whereas bending forces become significant in larger rotors with high Φ ratios. In this work, the bending stresses were neglected but a more accurate description of their influence will be carried out in future works.

A correct evaluation of the strut's dimensions is particularly important in small rotors due to the fact that a fast-rotating turbine often needs thick supporting struts to balance the centrifugal

stresses [24]. Similar struts, however, are characterized by a notable parasitic torque generation which causes a remarkable detriment of the overall performance of the machine.

In particular, in this study a constant shape of the struts was considered. In case of symmetrical airfoils, the same profiles were used. On the other hand, when the NACA4415 is used, the struts are supposed to be realized with the NACA0015 (same t/c ratio but straight camber). By these choices, a constant virtual drag coefficient [24] during the revolution was considered, whereas the dimensions of the struts were varied in Case 3 until the minimum ones which satisfied Eq. 7 were found. In detail, the chord of the struts (and consequently also the thickness, being the t/c ratio fixed) was calculated on the basis of the resistant area defined by Eq.7. When the calculated struts dimensions exceeded the chord of the blade, the struts number was increased by one for each blade and the new dimensions of each element were recalculated on the basis of the same procedure, in all the investigated configuration, a maximum struts' number of three was constantly observed. Finally, the effects of "bluff-section" struts was investigated, in order to stress more evidently the influence of the parasitic phenomena: the struts were assumed to have a constant virtual drag of 0.3 and a thickness varying with the same procedure described for the airfoil-shaped solutions.

4. Simulations and data reduction

The performance simulations of the machines were carried out with the *VARDAR* code of the Department of Industrial Engineering of the University of Florence. The code makes use of the Blade Element Momentum (BEM) Theory, by which the rotor performance is calculated coupling the momentum equation in the mainstream direction of the wind and a one-dimensional aerodynamic analysis of the interactions between the airfoils in motion and the oncoming flow on the rotor [20,33,38-39] by means of pre-calculated polars. Even if more advanced simulations techniques (including computational fluid dynamics) are today available for the simulation of VAWTs (e.g. [39-41]), BEM approaches are still the most widely exploited tools for the preliminary design of these rotors, as they provide sufficiently reliable

results in terms of global performance (whereas a poor description of the instantaneous flow field around the rotor is achieved) coupled with a notably reduced computational cost.

In particular, the VARDAR code has been specifically developed for H-Darrieus wind turbines using an improved version of a *Double Multiple Streamtubes Approach with Variable Interference Factors* [17,28,42] (Figure 4a). In this approach, the elementary torque for each azimuthal position is therefore given by Eq. 8:

$$T_{blade}(\vartheta) = F_t \cdot R = \frac{1}{2} \rho c W_{\vartheta}^2 C_{t(\vartheta)} R H \quad (8)$$

where C_t and W represent the tangential coefficient of the airfoil in the reference system of the rotating blade (Figure 4b) and the relative velocity of the flow experienced by the airfoil itself in the upwind or downwind half, respectively, expressed by Eqs. 9,10 and 11:

$$C_t = C_L \cdot \sin \alpha - C_D \cdot \cos \alpha \quad (9)$$

$$W_{up} = \sqrt{[(1-a) \cdot U_{\infty} \cdot \sin(\vartheta - \beta)]^2 + [(1-a) \cdot U_{\infty} \cos(\vartheta - \beta) + \omega R]^2} \quad (10)$$

$$W_{down} = \sqrt{[(1-a_2) \cdot U_{eq} \cdot \sin(\vartheta - \beta)]^2 + [(1-a_2) \cdot U_{eq} \cos(\vartheta - \beta) + \omega R]^2} \quad (11)$$

As for the more general Eq. 5, the relative speed is given by the sum of peripheral speed and wind speed, properly reduced by the induction factor (either upwind or downwind). The value U_{eq} in Eq. 25 indeed represents the wind equilibrium velocity between actuator disks (see Figure 4).

The Glauert's correction for the BEM theory has been taken into account with the most recent improvements, together with the corrections due to blades finite Aspect Ratio, using the Lanchester-Prandtl model. This aspect is of particular relevance in the present analysis, as it allows the designer to account for the increasing tip-losses connected to blades with small height to chord ratios.

In order to increase the accuracy of the aerodynamic estimations, a specific sub model to account for the dynamic stall has been provided, following the Paraschivoiu's adaptation to the

DMS approach described in; at the same time, the stream tube expansion along the flow path was considered. For additional details on the code please refer to Refs. [23,26,33,37,42-43].

The prediction capabilities of the VARDAR code have been validated during a several-years' experience in the design of three real H-Darrieus rotors, having swept areas of 1, 2.5 and 5 m², respectively, and two or three blades, either straight or helix-shaped. The 1:1 models of all the rotors (two made of reinforce plastic and one of painted aluminium alloy) were tested in different wind tunnels (both with closed and open-jet). In all cases, the code was able to correctly predict both the power curves at different wind speeds and the starting ramps of rotor and is then considered fully predictive for the turbine typology investigated in this study. For further details on the code validation please refer to Refs. [23,33,37,42].

In the present analysis, the code provided the power coefficient of each configuration at all the wind speeds between the cut-in and the cut-out. The characteristic power coefficient of the machines at each wind velocity was conservatively evaluated in correspondence with the calculated performance 0.2 points of TSR after the peak of the operating curve. A similar precaution is often applied in order to define a load curve aimed at preventing the turbine from operating in the unstable part of the functioning curve [11,24]. Moreover, it is worth noticing that the cut-in speed in each case was set to the wind speed for which a positive power coefficient is obtained. This is, in fact, a precautionary assumption, because the self-starting of an H-Darrieus rotor in real wind is often ensured for several starting positions even if the overall power coefficient over the revolution is negative [42,45].

In further detail, for each configuration in terms of swept area (i.e. the discrete variable of the problem) specific performance maps were created [26] corresponding to a given wind distribution. Each map (e.g. see Figure 5) contains the overall efficiency of energy conversion (η_{en}) of the specific rotor, defined as in Eq. 12 and 13.

$$\eta_{en} = \frac{\sum_{u=cut-in}^{cut-out} c_p(u) \cdot u^3 \cdot T(u)}{\sum_{u=cut-in}^{cut-out} u^3 \cdot T(u)} \quad (12)$$

$$T(u) = f(u) \cdot 8760 \quad (13)$$

Upon examination of the equations, it is worth pointing out that the energy conversion efficiency was defined as the annual energy yield of the turbine over the year (i.e. the real extracted power at each wind speed multiplied by the time fraction, in hours, during which that wind blows $T(u)$) on the theoretical energy contained in the wind itself.

Based on its definition, this indicator differs from the classical power coefficient and allows one to simultaneously take into account both the efficiency of the turbine at all the wind speeds expected over the year and the effects related to the starting and resistance capabilities of the rotor (due to the variable cut-in and cut-out velocities considered).

Finally, within each map, a numerical identification of the maximum was performed, with the constraints of neglecting design solutions which imply Blade's Aspect Ratios higher than 35: in case of excessive ratios between the height and the chord, the bending resistance of such a slender blade would be indeed very poor, making the selected solution practically unfeasible.

This procedure would finally lead to the definition of the geometrical features of the rotor ensuring the largest energy harvesting over a year for the attended load case, average wind speed in the site and imposed swept area of the rotor.

The whole data reduction procedure is summarized in Figure 6, while a complete overview on the results in terms of best design solutions can be find in the Appendix Section.

5. Results

5.1 Energy Efficiency maps interpretation

A typical Energy Efficiency map has been presented in Figure 5 (e.g. for a swept area of 4.0 m², NACA0018 airfoil, \bar{U} =5 m/s in Case 2). A linear interpolation was performed between the calculated points (see Table 1) in order to more precisely outline the contours.

It is readily noticeable that an optimum-design zone (white-colored in the figure) can be typically distinguished in the bottom side. This zone represents the combination of the Φ and ζ

parameters which ensures the best compromise in terms of functioning Reynolds numbers on the airfoil (high peripheral speeds and chords) and efficiency of the blades (high Aspect Ratios). Moreover, one can also notice that the efficiency is almost zero in the left side of the map, where the very small chords remarkably reduce the lift generation, and becomes lower also in the right-bottom corner of the map, where the turbine heights tend to zero.

As discussed, within each map a numerical identification of the maximum was performed in order to define the geometrical features of the rotor ensuring the largest energy harvesting over a year under the present design constraints.

5.2 Case 1 - Aerodynamics

From a general point of view, it is worth remembering that Case 1 configuration actually refers to a hypothetical solution of a fully aerodynamic relationship between the geometrical features of the rotor and the power performance. By doing so, the influence of the main aerodynamic design parameters can be readily argued and the functioning behaviors of machines having different areas can be directly compared.

The main outcome of the analysis of Case 1 is that an opposite behavior was found between cambered and uncambered airfoils in this configuration.

As an example of uncambered airfoils, Figure 7 reports the variation trends which describe the dependence of the optimal values of the most relevant design parameters from the average wind speed for the NACA0015 airfoil.

Upon examination of Figure 7, some relevant markups can be promptly made. In particular:

- The dimensionless parameters present the same trends even when different swept areas are considered, although numerical values differ from one configuration to another, confirming that scale effects must be taken into account.
- When the average wind speed in the site increases, the best solidity decreases constantly and the Aspect Ratio rises significantly, whereas the Shape Factor Φ increases for

medium-low average wind speeds and then becomes stable. As a general remark, however, the turbine tends to become slenderer by increasing the average wind speed.

- Focusing on the dimensional parameters, the aforementioned trend is basically obtained throughout a constant decrease of the blades' chord with the average wind speed increase (with a steeper trend for medium-low \bar{U} and a flatter trend with an increased \bar{U}). The turbine diameter and height have instead an opposite trend, with a decrease and an increase in the first part, respectively, followed by a constant trend in the second part.

The main aerodynamic implication of these results is that, when the average wind velocity experienced by the turbine is low (left side of the plots), the best design is that ensuring the highest local Reynolds numbers on the blade by means of the geometrical proportions. As a consequence, the chord values are maximized (see Eq. 1) at low wind speeds and then the solidity values are high (Eq. 3).

By increasing the average wind speed, the velocity triangles on the airfoils are altered thanks to the increased relative velocities experienced by the blades: the chords can be therefore reduced without decreasing the functioning Reynolds numbers. For high mean wind velocities, however, the chord length stops decreasing and more efficient blades (i.e. higher Aspect Ratios, $AR=H/c$ [20-21,24]) are obtained by means of an increase of the turbine height (black curves in the graphs on the left). The optimal solidity constantly decreases with \bar{U} .

Moreover, a well-defined dependence on the t/c ratio of the airfoil was observed. For example, in Figures 7 and 8 the optimal trends of the solidity and the blade's Aspect Ratio for the three uncambered airfoils are reported.

In detail, by decreasing the t/c ratio of the selected airfoil (Figure 8), i.e. from NACA0018 to NACA0015 and NACA0012, the optimal solidity of the turbine is constantly reduced. This phenomenon can be related to a decrease of the requested chord. This solution is indeed allowed by an increase of the target peripheral speed of the rotor which, on one hand, ensure a suitable Reynolds number on the airfoil (Eq.1) and, on the other hand, decreases the incidence

angles range: thinner airfoils (e.g. the NACA0012), although more efficient for high relative speeds, have indeed a lower stall angle and are generally more sensitive to incidence angle variations. Contemporarily (Figure 9), the same reasons induce an opposite behavior of the blade's Aspect Ratio (AR_b), which is constantly higher in case of thinner airfoils (the shorter chords are combined with an almost equal trend of optimal heights).

The optimal design trends in case of the cambered NACA4415 airfoil are notably different. In particular, whenever this typology of profile is applied, the scale effects due to the swept area become negligible, as the high C_L/C_D ratio of this airfoil [44] makes the dependence of the aerodynamic performance from the chord very low. The Aspect Ratio can then rise significantly to pursue the higher blade's efficiency. The optimal design proportions in Case 1 for the NACA4415 airfoil are reported in Figure 10. In this configuration, the optimal solidity is low (see Eq. 3) and the AR_b very high mainly due to the very short chords.

5.3 Case 2 - Limited centrifugal load

The results obtained from the examination of Case 1 are very useful to comprehend the aerodynamic trends connected to a variation of the wind velocities experienced by the turbine; structural constraints like the centrifugal load have, however, relevant impact on the best design compromise of a machine [24,26].

To this purpose, next figures report some results of the investigation on the study-cases in Case 2, in which a ζ_{lim_b} (Eq. 6) of 90 N/mm² was considered [26,33]; for a wider overview of the results, please see Appendix B.

First, it was noticed that, when the average wind velocities are low (i.e. 3÷4 m/s), the structural constraints actually do not affect the definition of the best design parameters; the operating rotational speeds at these velocities are low and the resulting centrifugal loads do not exceed the structural limits. In case of the NACA4415, the best design is once again imposed due to limitation on the blade's Aspect Ratio.

Once again, the two types of airfoils work differently. If the uncambered profiles are selected and the medium-high wind speeds become more frequent, the reduction of the solidity with the average wind speed noticed in Case 1 ceases (an almost constant value is reached – e.g. see Figure 11), mainly due to the stop in the decrease of the optimal chord (Figure 12).

This trend can be explained by considering that, when the wind velocities are high, the most suitable compromise in terms of energy-yield capabilities comes from a reduction of the peak efficiency of the turbine (higher solidity) which, however, implies a reduction of the operating rotational regime [24,26]. This reduction makes the centrifugal loads decrease and allows the turbine to extract energy from the wind with all the considered wind velocities.

In particular, after examining the Energy Efficiency maps (e.g. for the NACA0018, swept area $A=4\text{ m}^2$ in Figure 13), it is readily noticeable that, for low average wind speeds, the best efficiency zone first migrates towards lower solidities and higher Φ ratios. When the high wind speeds become more frequent, however, a new zone of best efficiency arises at higher ζ and Φ ratios.

On the other hand, in case the NACA4415 is adopted, the optimal design solution highlighted in Case 1 (small chords, very high AR_b and high revolution speeds) is no longer feasible due to the limitation to the centrifugal load.

As a result, the best solidity value is slightly increased for medium-high average wind speeds (Figure 14); contemporarily, the chords and diameters remarkably increase in order to achieve a drastic reduction of the revolution speed (Figure 15). One should indeed remember that longer chords ensure more favorable Reynolds numbers on the airfoil without increasing the relative speed (see Eq. 3), whereas higher diameters act oppositely by improving the relative speed (Eq. 4) or, conversely, ensure the same relative speed with lower revolution speeds.

Finally, it is also worth noticing that this increase of the diameter for high average wind speeds is avoided only for high swept areas (i.e. $A=9.0\text{ m}^2$), where the limit on the centrifugal load is

mitigated by the large diameters. In these conditions, the AR_b can be also slightly increased, with a partial recovery of the blades' efficiency (see Appendix B).

5.4 Case 3 - Centrifugal load and struts' parasitic torque

Focusing now on a real-type machine, a further constraint must be included in the identification of the best design trends: the parasitic torque of the struts is, in fact, a key element in defining both the peak efficiency of the machine and its functioning behaviour at different wind speeds. Due to the relevance of this load case, the complete comparison of the optimal design configurations was reported in Appendix D.

The calculations showed that the general effect of the parasitic torque is to slightly flatten the trends of the design parameters as a function of the average wind speed. The best design solutions tend in fact to collapse in the configurations that minimize the contribution of the parasitic components [26]. The general tendencies described in Section 4.3 are, however, still of validity and will not be all again discussed. In particular, the efficiency maps shape discussed in Figure 13 was confirmed also under this load case, with the only discussed restriction of the high-efficiency zone. Some interesting remarks can however be made.

First, Figure 16 reports the comparison between the optimal solidity trends in Case 2 and 3 for NACA0012 and NACA0018 airfoils (swept area of 1.0 m^2), as a function of the average wind speed. As one may notice, no great difference stands between the two cases when the average wind speed in the site is sufficiently high (i.e. higher than 5 m/s). Conversely, in case of low average wind speeds, the optimal solidity in Case 3 is higher than that obtained in case the parasitic torque is neglected.

In order to give a correct interpretation of the results, it is worth remembering that the parasitic torque generated by the rotating structures which do not contribute to the torque generation (e.g. struts, tie-rods, etc.), has a quadratic dependence on the rotational speed of the rotor (directly affecting the tangential velocity) and a lighter and more complex dependence on the wind velocity (see Refs. [33,36]).

Based on these considerations, one can understand that, when the wind speeds are low, the impact of the parasitic torque on the effective energy-extraction capability of the rotor is more relevant: as a consequence, the optimal design tends to increase the solidity, in order to achieve a reduction of the revolution regime [24].

Focusing on the cambered airfoil, the situation is again quite different (see Figure 17). With this airfoil selection, which is thought to provide a good torque production even in low winds, the best design solution is almost unaltered within $\bar{U}=5$ m/s with respect to Case 2.

When the high wind speeds in the site become more frequent, however, the “low solidity” solutions, which are associated with very high revolution speeds, are not suitable anymore, as the parasitic torque has become too high. The optimal solutions hence tend to higher solidities (i.e. slower revolution speeds), very similar to those identified for the uncambered airfoils.

Finally, in order to further stress the importance of the parasite torque of the struts, in Figure 18 a comparison between the optimal solidity for a turbine with the NACA0012 airfoil and a swept area of 1 m^2 is reported as a function of the strut’s shape. In detail, when the drag of the struts increases, the solidity tends to notably increase, in the attempt of reducing the revolution speed of the rotor. In the selected case, the more energy-efficient solution would be very solid (even up to the limit of $\sigma = 0.6$), which is, however, a practically unfeasible solution. In a similar case, a compromise must be pursued in practically designing the rotor, including a reduction of the effective energy-yield capabilities.

At the end of this study, one could then conclude that, from an energy viewpoint, future design of medium and small-size Darrieus rotors should be based on the maximization of the energy yield on the basis of the characteristics of the potential installation site. In particular, for given rotor’s dimensions, a differently shaped turbine would be about to be preferred as a function of the average wind speed of the installation. For example, in Figure 19 the optimal design choices for a turbine having a swept area of 4 m^2 and equipped with NACA0018 airfoils are presented as a function of the average wind speed in the site. In particular, the

aforementioned trends in terms of increase of the H/D ratio and decrease of the chord length are clearly distinguishable.

For the same family of turbines (presented trends are consistent with all the analyses presented in this study), the annual energy yield of the optimized rotors is presented in Figure 20 as a function of the average wind speed in the site. In order to provide a sensitivity analysis on the benefits of the proposed approach, in the same figure the energy yield increase with respect to two others design choices is presented. In further details, Study Turbine A represents a hypothetical turbine designed to have the maximum efficiency at 6 m/s, which could be, for example, the average speed in the site [23]. Study Turbine B instead represents the turbine optimized by means of the maximum-energy-yield criterion at $\bar{U}=6$ m/s.

Some very interesting remarks can be done. First, it is worth noticing that a design approach based on the maximum annual energy yield actually provides an increase of performance in all cases. In particular, focusing on the 6 m/s bar, one can notice that benefits can be achieved also in comparison to a design criterion based on the same average speed of the site.

Moreover, the proposed criterion is able to provide notable energy increase (up to 10% in the present case) when the wind speeds in the site are low, confirming the prospects of specific future design choices for these conditions.

6. Conclusions

In this study, a numerical analysis has been carried out to define some design guidelines for Darrieus wind turbines aimed at optimizing the annual energy yield of each machine in the installation site. The main outcomes of the analysis can be summarized as follows.

Focusing on the only aerodynamic requirements, an opposite behavior was found between cambered and symmetric, uncambered airfoils. For uncambered profiles, when the average wind speed in the site increases, the best solidity decreases constantly, the Aspect Ratio rises significantly, whereas the Shape Factor Φ increases for medium-low average wind speeds and then becomes stable. This trend is mainly due to the fact that, by increasing the wind speed, the

relative velocity is increased, and the Reynolds number is improved. The chords can be then reduced, with notable benefits in terms of blade's efficiency. A well-defined dependence on the t/c ratio was also observed: by decreasing the t/c ratio, the optimal solidity is constantly lower whereas higher Aspect Ratios are preferable. When a cambered airfoil is instead selected, the scale effects due to the swept area becomes negligible, as the high C_L/C_D ratio of this airfoil makes the dependence of the aerodynamic performance from the chord very low, hence allowing the Aspect Ratio to rise significantly to pursue the higher blade's efficiency. With this selection, the optimal solidity is consequently also very low.

On the other hand, when structural constraints and notable parasitic contributions are introduced, the best configurations when the average wind velocities are low are similar to that coming from the aerodynamic analysis, although the optimal design generally tends to increase the solidity, in order to ensure a better functioning conditions to the airfoils (higher Reynolds numbers, increased torque) and contemporarily achieve a reduction of the revolution regime, which contains the parasitic torque. On the other hand, when the medium-high wind speeds become more frequent, the most suitable compromise in terms of energy-yield capabilities generally comes from a reduction of the peak efficiency of the turbine which, however, ensures a good energy extraction is a wider range of functioning conditions. In case of uncambered airfoils, in particular, this goal is obtained with a general increase of the optimal solidity, which makes the revolution speed decrease and allows the turbine to extract energy from the wind with all the considered wind velocities. As a general remark, however, by increasing the parasitic contributions, the transition of the best design compromise to higher solidity solutions is anticipated, due to the stronger dependence of the performance on the rotational speed.

At the end of this work, it has to be noticed that the present analysis was carried out under specific assumptions in terms of dimensions, airfoil types, load system and struts' shape; on these bases, the reader has to consider that different performance maps could come from a new set of theoretical assumptions, although some general trends outlined in the work (e.g. the

579 influence of the turbine proportions on the Reynolds numbers and the rotational speed) are of
580 general validity.

581 The proposed design criterion, however, besides being theoretically more rigorous from a
582 truly energetic point-of-view than a conventional one based on a single reference wind speed,
583 has shown interesting prospects in terms of energy production improving. In particular,
584 different models could be designed for specific wind distributions in order to optimize the
585 energy yield also at low wind speeds, which are very frequent in several countries and in
586 unconventional installation sites, e.g. the urban environment.

587 **Nomenclature**

588	A	Swept Area	$[m^2]$
589	a	Induction Factor	
590	AR	Aspect Ratio	
591	c	Blade Chord	$[m]$
592	C_D	Drag Coefficient	
593	C_L	Lift Coefficient	
594	C_t	Tangential Force Coefficient	
595	c_p	Power Coefficient	
596	D	Turbine Diameter	$[m]$
597	F_n	Normal Force on the Blade	$[N]$
598	F_{ST}	Force due to Centrifugal Loads	$[N]$
599	F_t	Tangential Force on the Blade	$[N]$
600	f	Frequency	
601	H	Turbine Height	$[m]$
602	m	Mass	$[kg]$
603	N	Blades/Struts Number	
604	P	Power	$[W]$

605	R	Turbine Radius	[m]
606	Re_c	Chord-based Reynolds Number	
607	T	Annual Time of each Wind Class	[h]
608	t	Airfoil Thickness	[m]
609	TSR	Tip-Speed Ratio	
610	u	Wind Class	[m/s]
611	U_∞	Absolute Wind Speed	[m/s]
612	\bar{U}	Average Wind Speed	[m/s]
613	W	Relative Wind Speed	[m/s]
614			
615	<u>Superscripts</u>		
616	*	Per Unit Area	
617	\rightarrow	Vectorial Quantity	
618			
619	<u>Subscripts</u>		
620	air	Air	
621	b	Blade	
622	en	Energy	
623	eq	Equilibrium (between upwind and downwind)	
624	res	Resistant Component	
625	ST	Struts	
626			
627	<u>Greek letters</u>		
628	Φ	Turbine Shape Factor	
629	α	Incidence Angle on the Airfoils	[deg]
630	β	Pitch Angle	[deg]
631	η_{en}	Energy-conversion Efficiency	

632	ν	Kinematic Viscosity	[m ² /s]
633	ζ	Chord/Diameter Ratio	
634	ρ	Air Density	[kg/m ³]
635	σ	Solidity	
636	ς	Structural Stress	[N/m ²]
637	ω	Rotational Speed	[rad/s]

638 **References**

- 639 [1] Global Wind Report. Global Wind Energy Council; 2011.
- 640 [2] Global Wind Energy Outlook. GWEC, Brussels (Belgium); 2011.
- 641 [3] Oceans of Opportunity. EWEA, Brussels (Belgium); 2009.
- 642 [4] Junginger M, Faaij A, Turkenburg WC. Cost Reduction Prospects for Offshore Wind
643 Farms. Wind Engineering 2004;28(1):97–118.
- 644 [5] Kirke BK, Evaluation of self-starting vertical axis wind turbines for standalone
645 applications. Ph.D. thesis, Griffith University, Gold Coast (Australia); 1998.
- 646 [6] Small Wind Turbine Global Market Study. AWEA, Whashington DC (USA); 2008.
- 647 [7] Mertens S. Wind Energy in the Built Environment. Brentwood (UK): Multi-Science; 2006.
- 648 [8] Dayan E. Wind energy in buildings: Power generation from wind in the urban environment
649 - where it is needed most. Refocus 2006;72(2):33-38.
- 650 [9] Beller C. Urban Wind Energy - State of the Art 2009, Risø Laboratory - DTU, Roskilde
651 (Denmark), Tech. rep. Risø-R-1668(EN); 2009.
- 652 [10] Balduzzi F, Bianchini A, Ferrari L. Microeolic turbines in the built environment: influence
653 of the installation site on the potential energy yield. Renewable Energy 2012;45:163-174.
- 654 [11] Balduzzi F, Bianchini A, Carnevale EA, Ferrari L, Magnani S. Feasibility analysis of a
655 Darrieus vertical-axis wind turbine installation in the rooftop of a building. Applied Energy
656 2012;97:921–929.

657 [12] Syngellakis K. Urban wind turbines: Development of the UK market. Proc. of the
658 European Wind Energy Conference 2006, February 27-March 2, Athens (Greece); 2006.

659 [13] Banks D, Cochran B, Denoon R., Wood G. Harvesting Wind Power from Tall Buildings.
660 Proc. of the CTBUH 8th World Congress, Dubai (UAE), 2008 In: Chicago: Council on Tall
661 Buildings and Urban Habitat; 2008, pp. 320-327.

662 [14] Sarma NK, Biswas A, Misra RD. Experimental and computational evaluation of Savonius
663 hydrokinetic turbine for low velocity condition with comparison to Savonius wind turbine at
664 the same input power. Energy Conversion and Management 2014;83:88-98.

665 [15] Roy S, Saha UK. Review of experimental investigations into the design, performance and
666 optimization of the Savonius rotor. Proc. of the Institution of Mechanical Engineers, Part A:
667 Journal of Power and Energy 2013;227(4):528-542.

668 [16] Gupta R, Biswas A, Sharma KK, Comparative study of a three-bucket Savonius rotor with
669 a combined three-bucket Savonius-three-bladed Darrieus rotor. Renewable Energy 2008;33(9):
670 1974-1981.

671 [17] Mertens S, van Kuik G, van Bussel G. Performance of an H-Darrieus in the Skewed Flow
672 on a Roof. Journal of Solar Energy Engineering 2003;125:433-440.

673 [18] Simão Ferreira CJ, van Bussel G, van Kuik G. An analytical method to predict the
674 variation in performance of a H-Darrieus in skewed flow and its experimental validation. Proc.
675 of the European Wind Energy Conference, February 27-March 2, 2006, Athens (Greece); 2006.

676 [19] Bianchini A, Ferrara G, Ferrari L, Magnani S, An improved model for the performance
677 estimation of an H-Darrieus wind turbine in skewed flow. Wind Engineering 2012;36(6):667-
678 686.

679 [20] Paraschivoiu I, Wind Turbine Design with Emphasis on Darrieus Concept. Polytechnic
680 International Press, Canada; 2002.

681 [21] Bianchini A, Ferrari L, Magnani S. Analysis of the Influence of Blade Design on the
682 Performance of an H-Darrieus Wind Turbine. Proc. ASME-ATI-UIT 2010 Conference on
683 Thermal and Environmental Issues in Energy Systems, Sorrento (Italy) May 16-18; 2010.

684 [22] Sharpe T, Proven G. Crossflex: Concept and early development of a true building
685 integrated wind turbine. Energy and Buildings 2010;42:2365-2375.

686 [23] Bianchini A, Ferrari L, Schneider A. First steps in the design and optimization of Darrieus
687 VAWTs for microeolic applications. Proc. World Renewable Energy Congress (WREC) X,
688 Glasgow (Scotland), July 19-25; 2008.

689 [24] Ferrari L, Bianchini A. Critical aspects in the design of a small-size Darrieus wind turbine.
690 Proc. World Renewable Energy Congress (WREC) XI, Abu Dhabi (UAE) September 25-30;
691 2010.

692 [25] Aslam Bhutta MM, Hayat N, Farooq AU, Ali Z, Jamil ShR, Hussain Z, Vertical axis wind
693 turbine – A review of various configurations and design techniques. Renewable and
694 Sustainable Energy Reviews 2012;16(4):1926-1939.

695 [26] Bianchini A, Ferrari L, Magnani S. Energy-yield-based optimization of an H-Darrieus
696 wind turbine. Proceedings of the ASME Turbo Expo 2012, Copenhagen (Denmark), June 11-
697 15; 2012.

698 [27] Manwell JF, McGowan JG, Rogers AL. Wind Energy Explained, 2nd edition, Wiley,
699 U.K.; 2009.

700 [28] Justus CG, Hargraves WR, Mikhail A, Graber D. Methods for estimating wind speed
701 frequency distributions. Journal of Applied Meteorology 1978;17(3):350-353.

702 [29] Akdağ SA, Dinler A. A new method to estimate Weibull parameters for wind energy
703 applications. Energy Conversion and Management 2009;50(7):1761-1766.

704 [30] Freitas de Andrade C, Maia Neto HF, Costa Rocha PA, Vieira da Silva ME. An efficiency
705 comparison of numerical methods for determining Weibull parameters for wind energy

706 applications: A new approach applied to the northeast region of Brazil. *Energy Conversion and*
707 *Management* 2014;86(10):801-808.

708 [31] Bhuyan S, Biswas A. Investigation on self-starting and performance characteristics of
709 simple h and hybrid H-Savonius vertical axis wind rotors. *Energy Conversion and Management*
710 2014;87:859-867.

711 [32] Gupta R, Das R, Sharma KK. Experimental study of a Savonius-Darrieus wind machine.
712 In *Proceedings of the International Conference on Renewable Energy for Developing*
713 *Countries*, University of Columbia, Washington DC, 2006.

714 [33] Bianchini A. Performance Analysis and Optimization of a Darrieus VAWT. PhD Thesis,
715 School of Energy Engineering and Innovative Industrial Technologies, University of Florence
716 (Italy); 2011.

717 [34] Islam M, Ting D, Fartaj A, Desirable Airfoil Features for Smaller-Capacity Straight-
718 Bladed VAWT. *Wind Engineering* 2007;31(3):165–196.

719 [35] Klimas PC. Tailored Airfoils for Vertical Axis Wind Turbines. Sandia National
720 Laboratories, Albuquerque, N.M., SAND 84-1062; 1984.

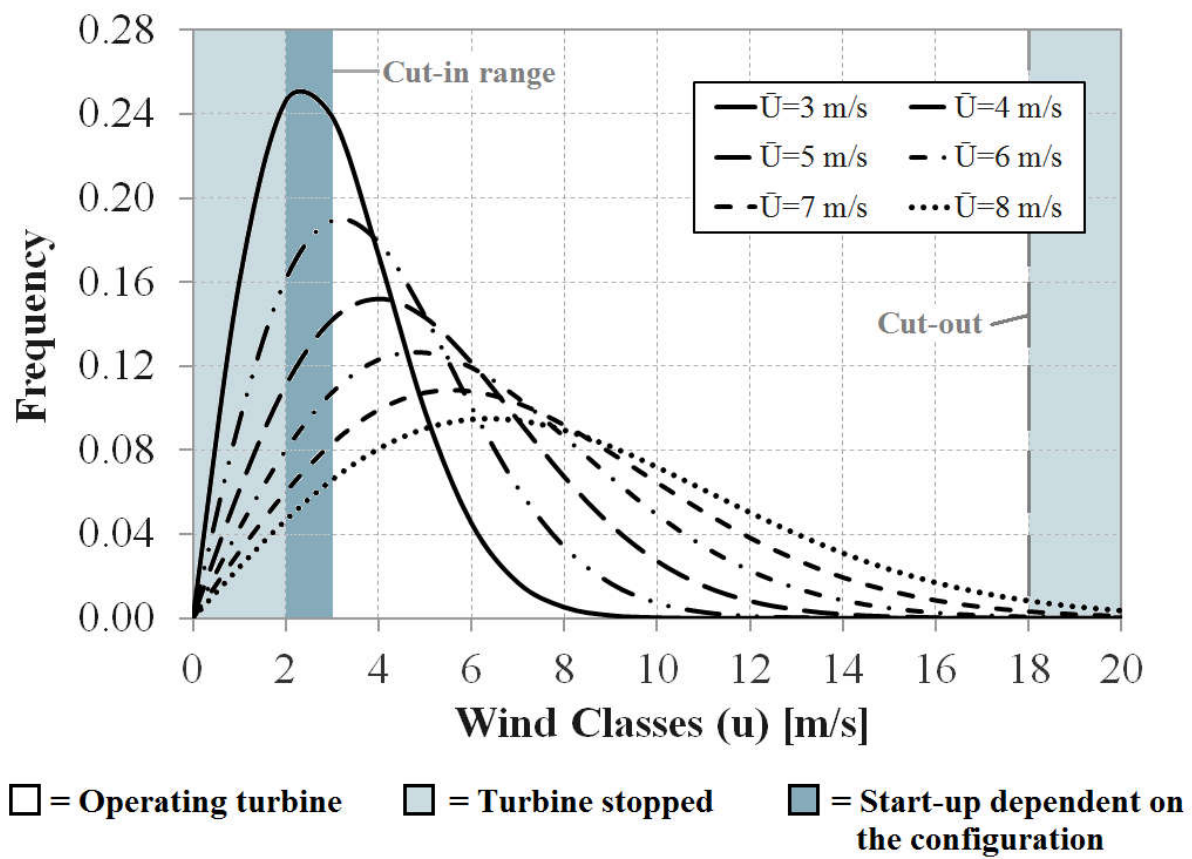
721 [36] Paraschivoiu I, Delclaux F. Double Multiple Streamtube Model with Recent
722 Improvements. *Journal of Energy* 1983;7(3):250-255.

723 [37] Balduzzi F, Bianchini A, Maleci R, Ferrara G, Ferrari L. Blade design criteria to
724 compensate the flow curvature effects in H-Darrieus wind turbines. *Journal of Turbomachinery*
725 2015;137(1):1-10.

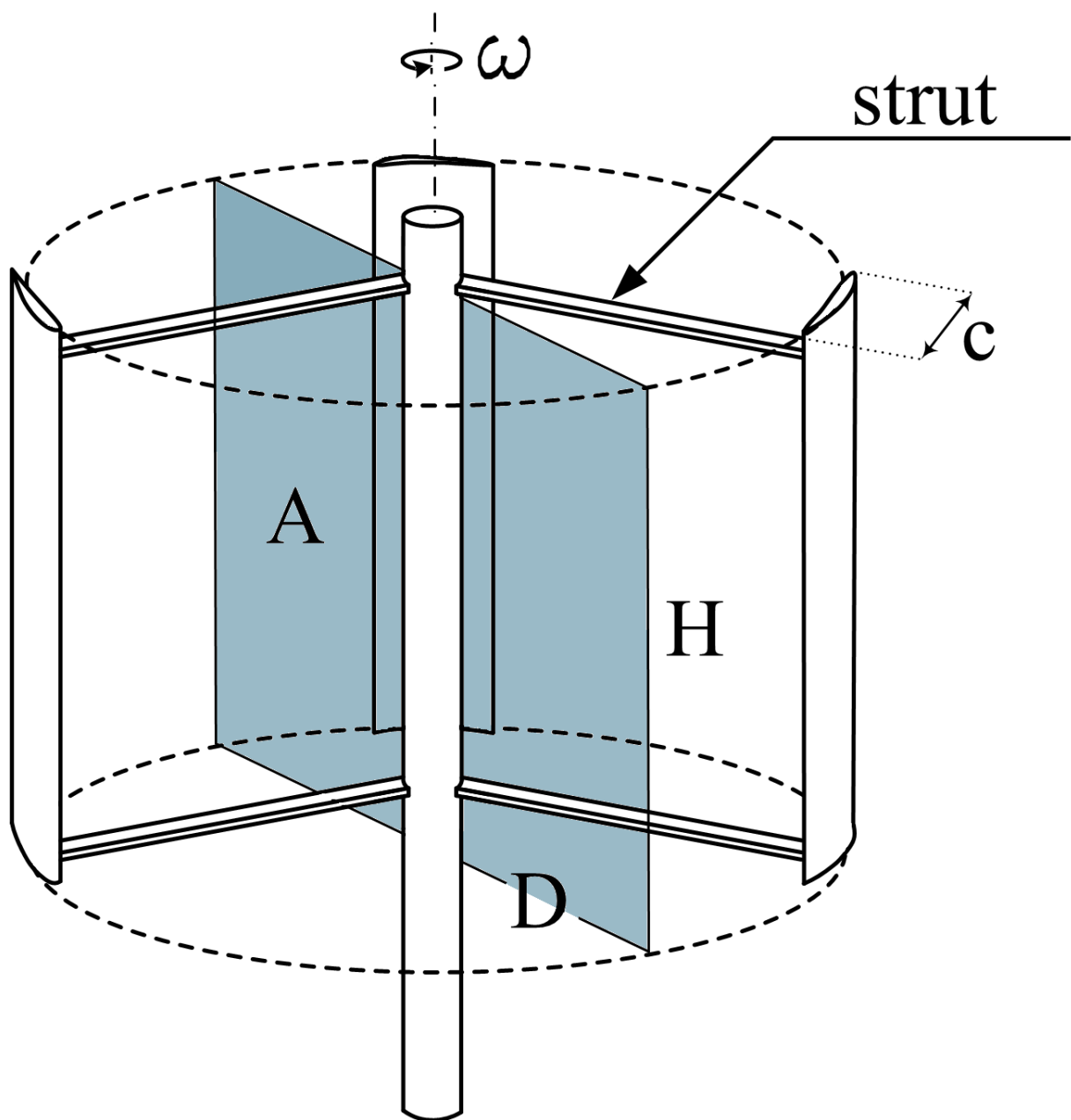
726 [38] Camporeale SM, Magi V. Streamtube model for analysis of vertical axis variable pitch
727 turbine for marine currents energy conversion. *Energy conversion and Management*
728 2000;41(16):1811-1827

729 [39] Islam M, Ting D SK, Fartaj A. Aerodynamic models for Darrieus-type straight-bladed
730 vertical axis wind turbines. *Renewable and Sustainable Energy Reviews* 2008;12:1087-1109.

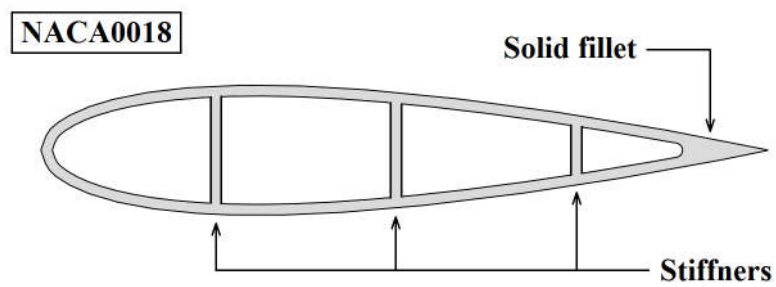
- [40] Wang LB, Zhang L, Zeng ND. A potential flow 2-D vortex panel model: Applications to vertical axis straight blade tidal turbine. *Energy Conversion and Management* 2007;4(2):454-461.
- [41] Simão Ferreira CJ. The near wake of the VAWT: 2D and 3D views of the VAWT aerodynamics. PhD Thesis, Technische Universiteit Delft, The Netherlands, 2009.
- [42] Bianchini A, Ferrari L, Magnani S. Start-up behavior of a three-bladed H-Darrieus VAWT: experimental and numerical analysis. *Proc. of the ASME Turbo Expo 2011, Vancouver (Canada), June 6-10; 2011.*
- [43] Bianchini A, Ferrari L, Carnevale E.A.. A model to account for the Virtual Camber Effect in the Performance Prediction of an H-Darrieus VAWT Using the Momentum Models. *Wind Engineering* 2011;35(4):465-482.
- [44] Ostowari C, Naik D. Post stall studies of untwisted varying aspect ratio blades with an NACA 4415 airfoil section - Part I. *Wind Engineering* 1984;8(3):176-194.
- [45] Dominy R, Lunt P, Bickerdyke A, Dominy J. Self-starting capability of a Darrieus turbine. *Proc. IMechE 221 Part A: Journal of Power and Energy* 2007:111-120.



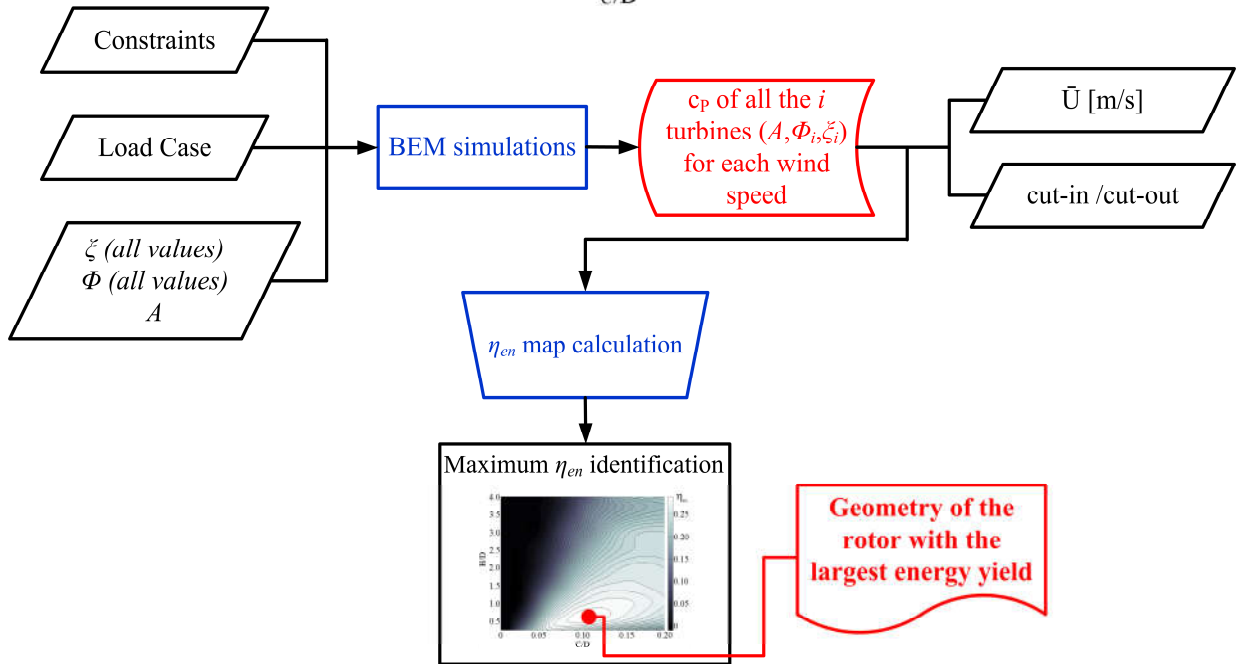
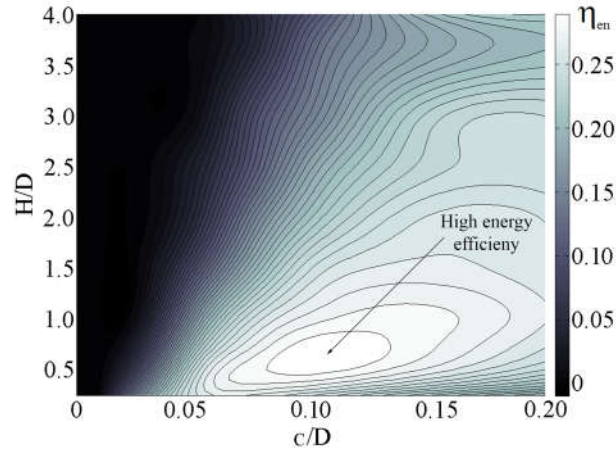
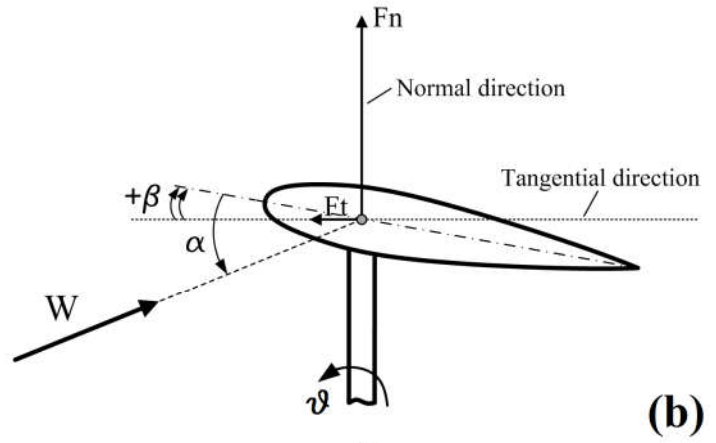
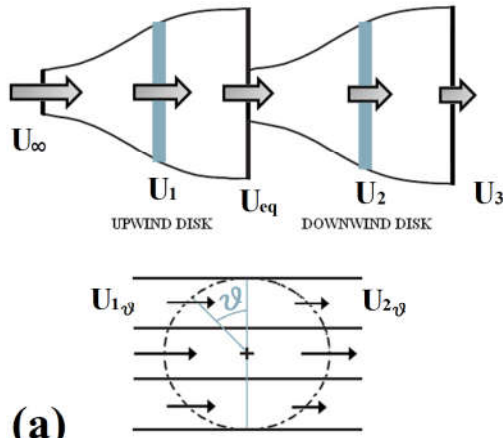
757

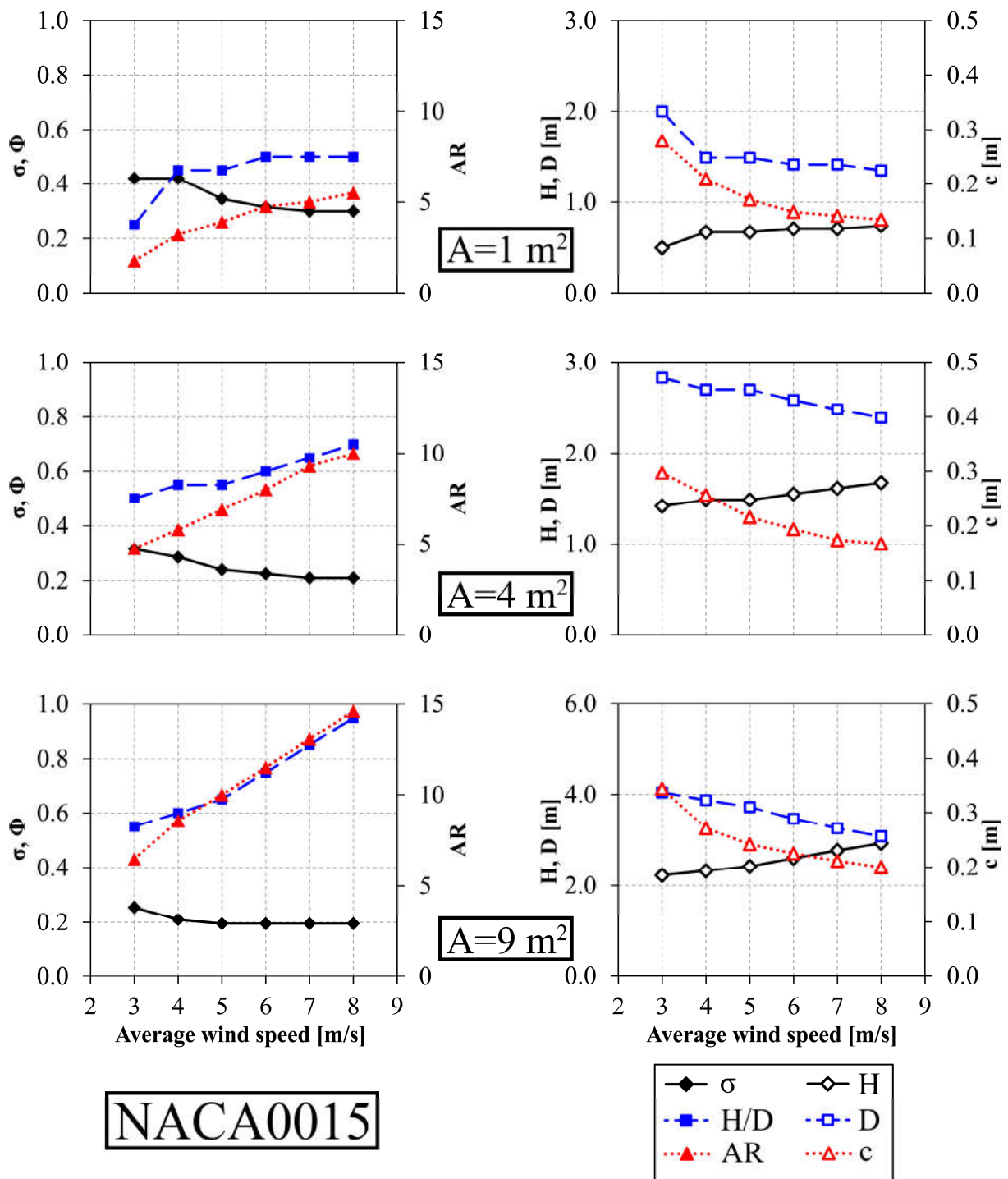


758

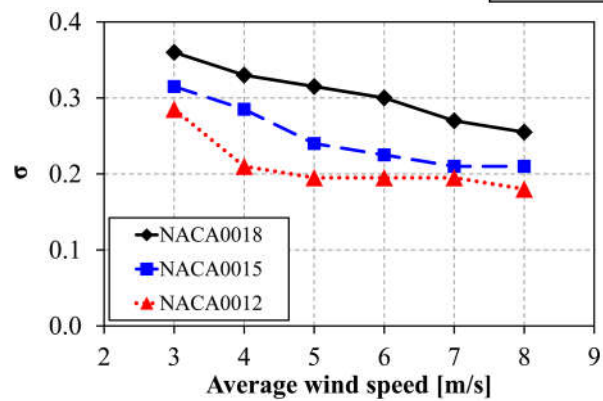


759

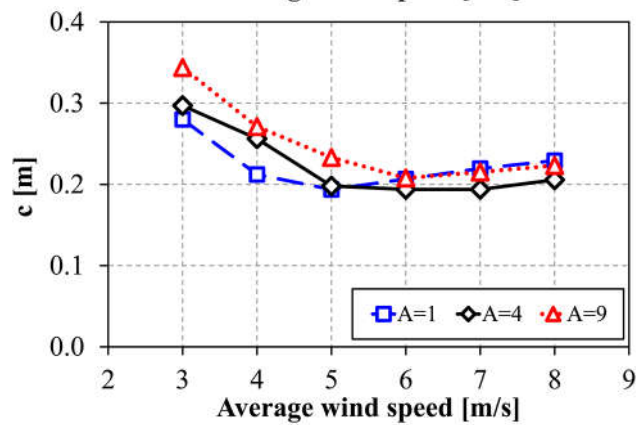
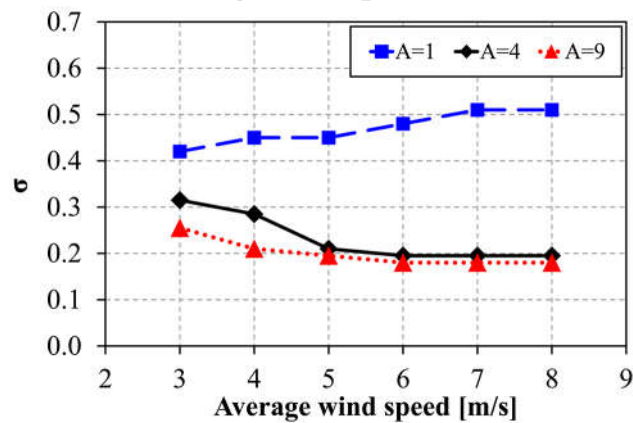
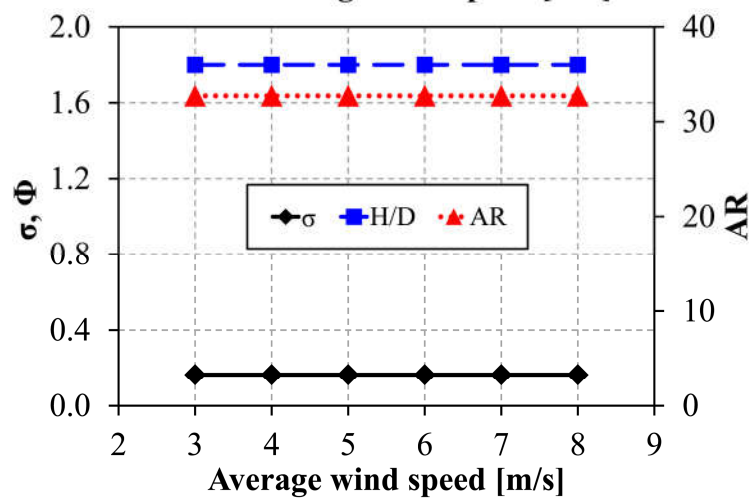
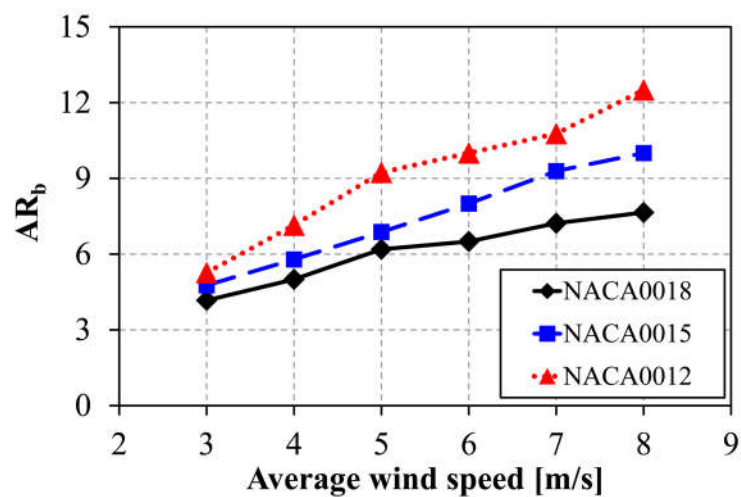


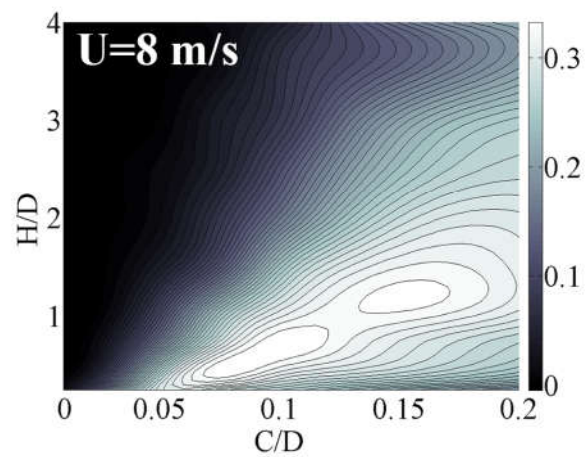
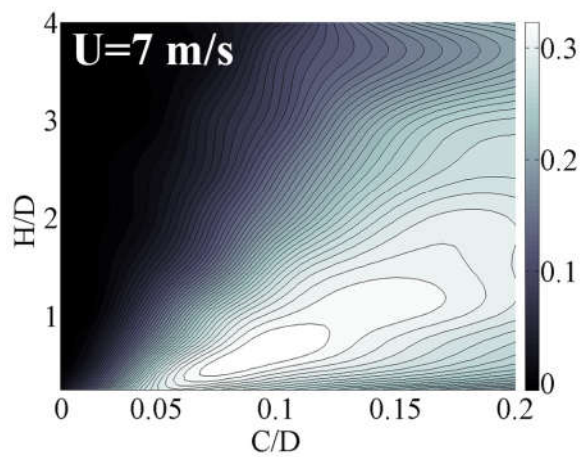
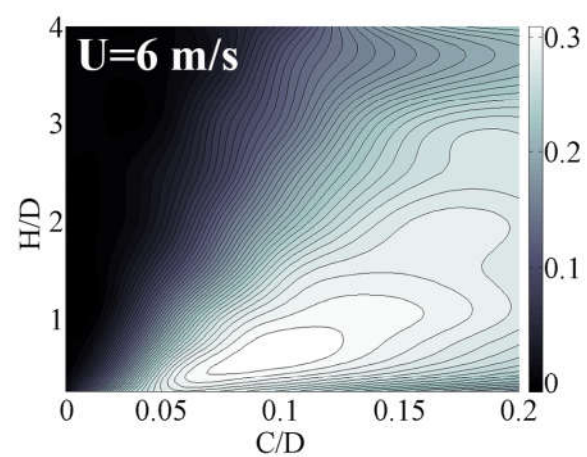
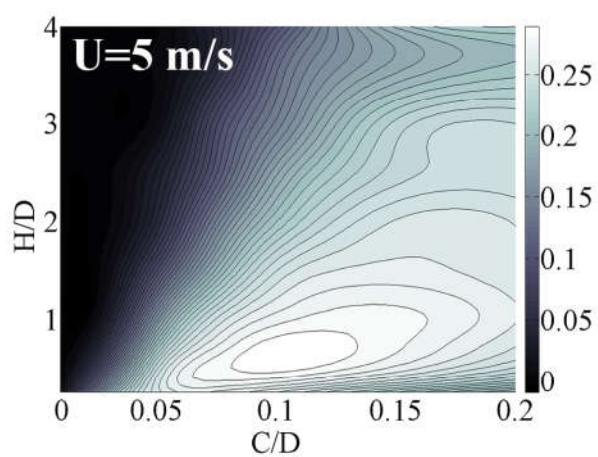
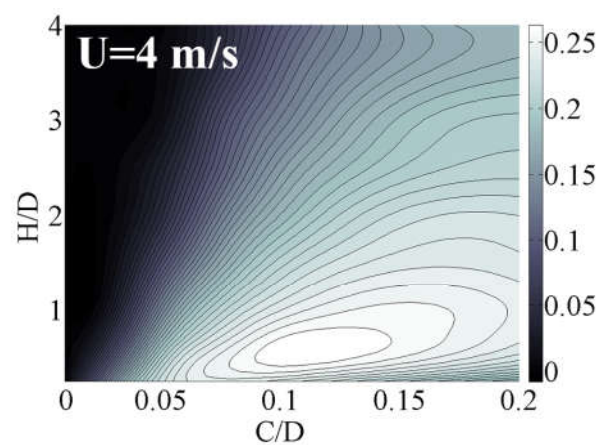
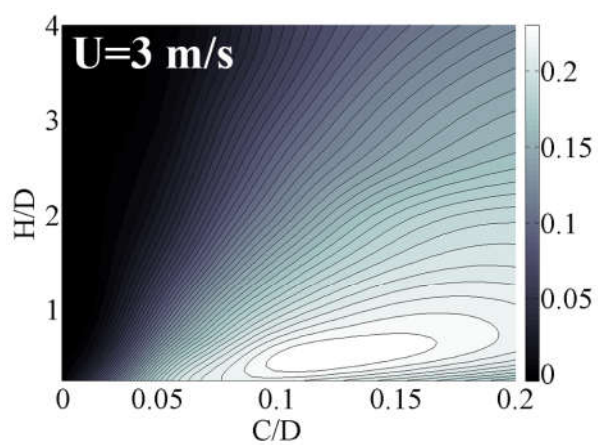


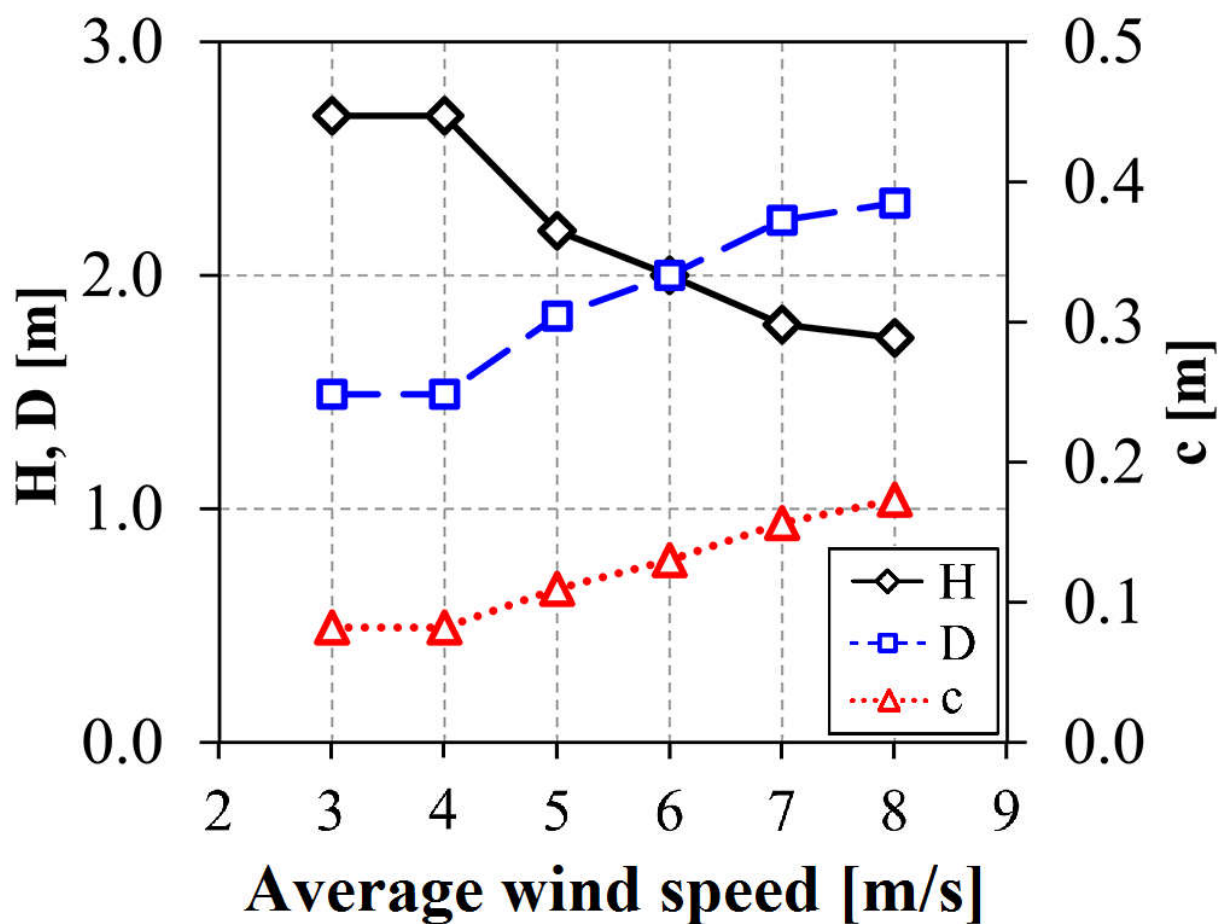
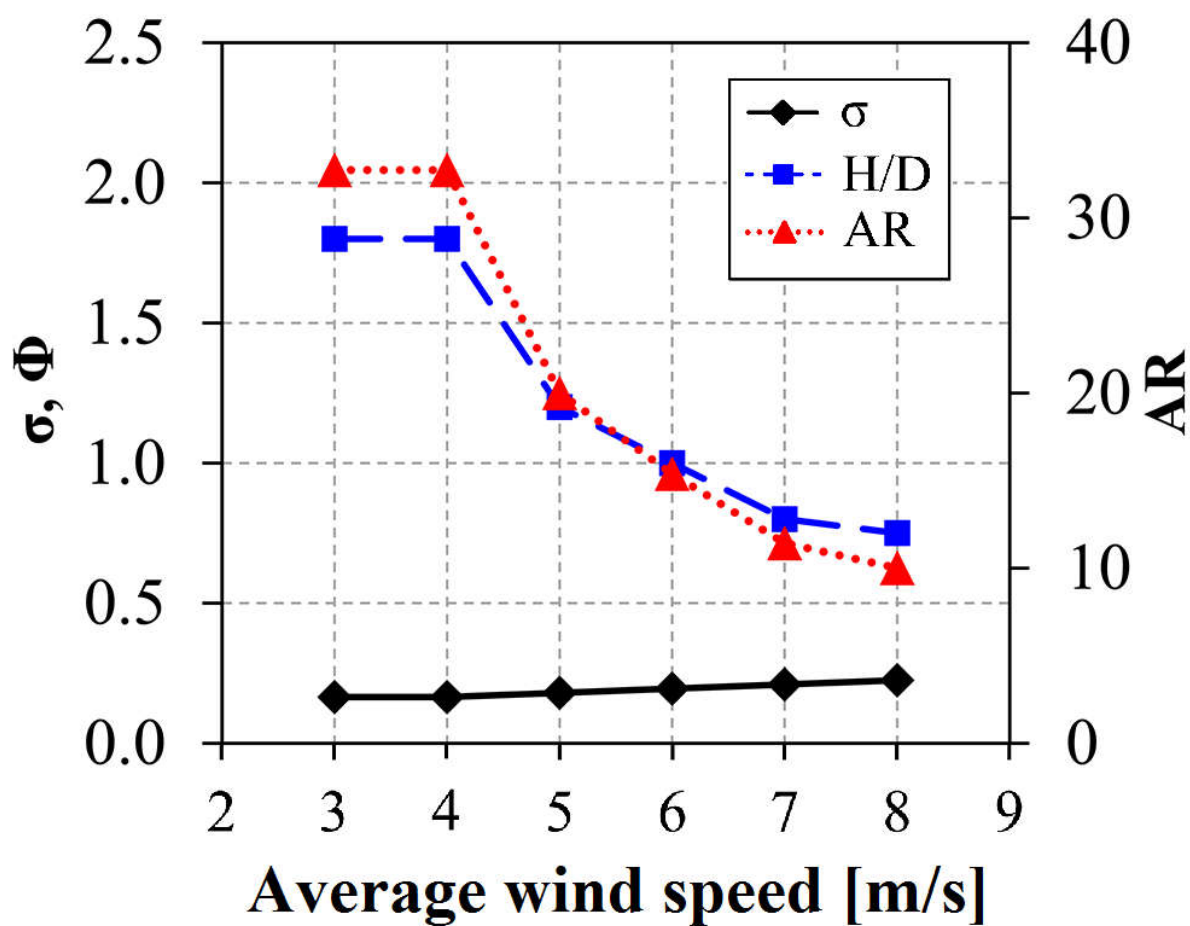
763

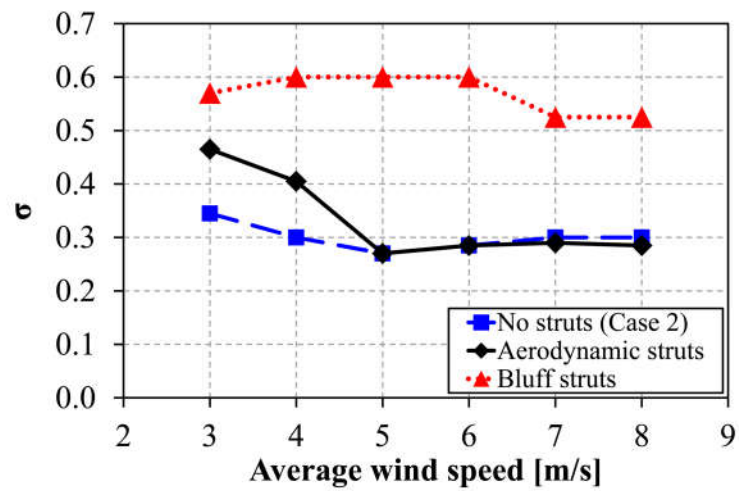
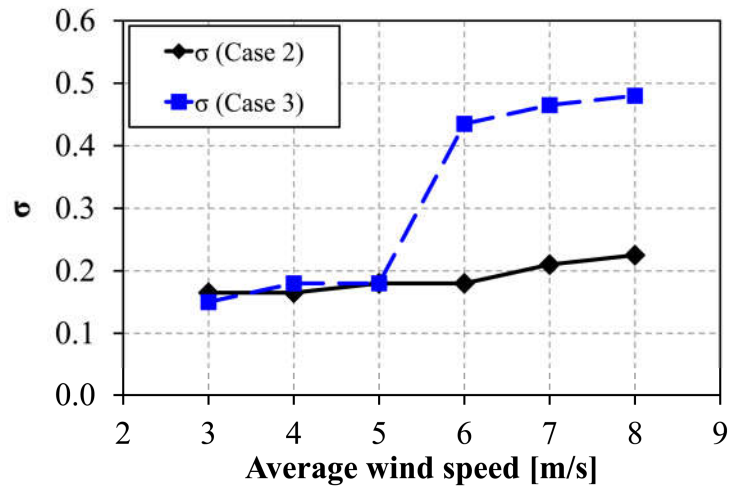
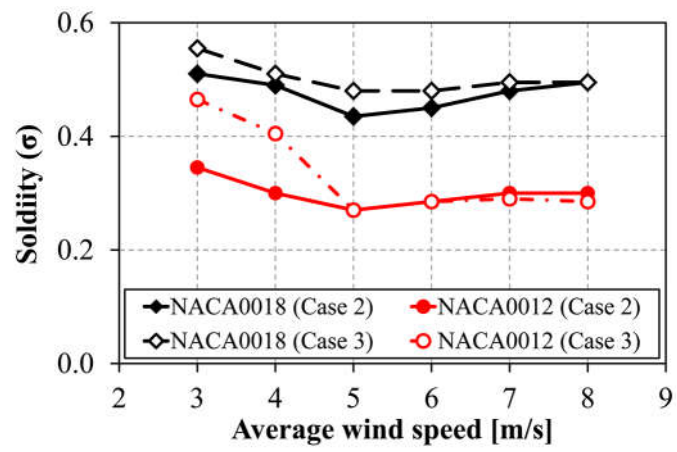


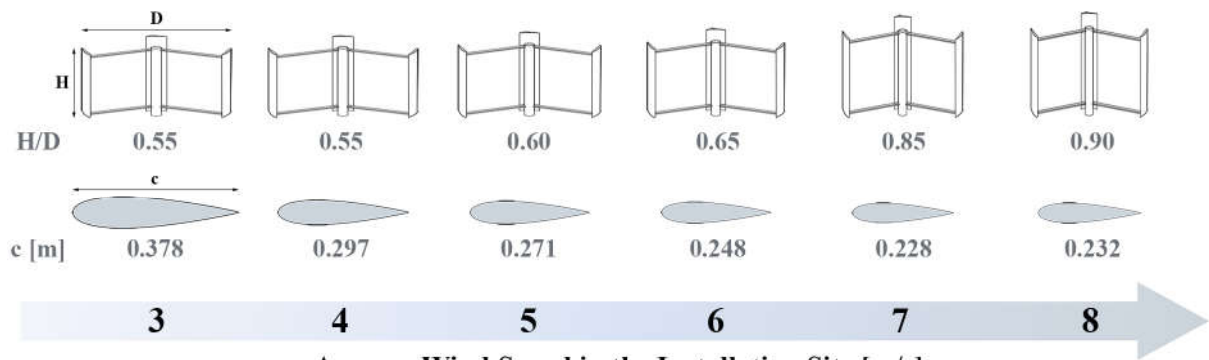
764



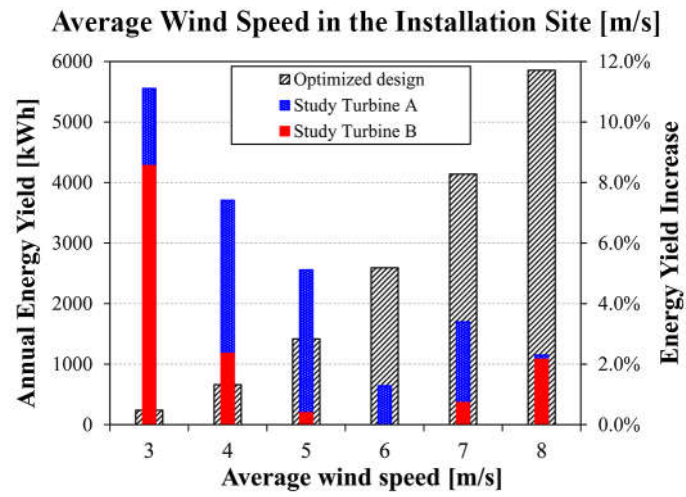








775



776